



# The Optimal Target and Connectivity for Deep Brain Stimulation in Lennox–Gastaut Syndrome

Aaron E.L. Warren, PhD <sup>1,2,3</sup> Linda J. Dalic, FRACP <sup>1,4</sup> Kristian J. Bulluss, PhD,<sup>5,6,7</sup>  
Annie Roten BAppSci,<sup>4</sup> Wesley Thevathasan, DPhil,<sup>4,5</sup> and John S. Archer, PhD<sup>1,2,3,4</sup>

**Objective:** Deep brain stimulation (DBS) can reduce seizures in Lennox–Gastaut syndrome (LGS). However, little is known about the optimal target and whether efficacy depends on connectivity of the stimulation site. Using outcome data from the ESTEL trial, we aimed to determine the optimal target and connectivity for DBS in LGS.

**Methods:** A total of 20 patients underwent bilateral DBS of the thalamic centromedian nucleus (CM). Outcome was percentage seizure reduction from baseline after 3 months of DBS, defined using three measures (monthly seizure diaries, 24-hour scalp electroencephalography [EEG], and a novel diary-EEG composite). Probabilistic stimulation mapping identified thalamic locations associated with higher/lower efficacy. Two substitute diffusion MRI datasets (a normative dataset from healthy subjects and a “disease-matched” dataset from a separate group of LGS patients) were used to calculate structural connectivity between DBS sites and a map of areas known to express epileptic activity in LGS, derived from our previous EEG-fMRI research.

**Results:** Results were similar across the three outcome measures. Stimulation was most efficacious in the anterior and inferolateral “parvocellular” CM border, extending into the ventral lateral nucleus (posterior subdivision). There was a positive association between diary-EEG composite seizure reduction and connectivity to areas of a *priori* EEG-fMRI activation, including premotor and prefrontal cortex, putamen, and pontine brainstem. In contrast, outcomes were not associated with baseline clinical variables.

**Interpretation:** Efficacious CM-DBS for LGS is linked to stimulation of the parvocellular CM and the adjacent ventral lateral nucleus, and is associated with connectivity to, and thus likely modulation of, the “secondary epileptic network” underlying the shared electroclinical manifestations of LGS.

ANN NEUROL 2022;92:61–74

Deep brain stimulation (DBS) is an emerging therapy for drug-resistant epilepsy. It involves implantation of electrodes into subcortical structures with the goal of modulating both the stimulation site and connected circuits generating seizures. In other diseases, particularly movement disorders, significant gains have been made in understanding optimal DBS targets,<sup>1</sup> distributed network effects of stimulation,<sup>2</sup> and connectivity predictors of efficacy.<sup>3</sup> However, comparatively little is known about the

optimal targets and connectivity for DBS in epilepsy, impeding broader therapeutic uptake.

Lennox–Gastaut syndrome (LGS) is a childhood-onset epilepsy associated with frequent seizures, severe cognitive impairment, and high burden of care.<sup>4</sup> LGS is a quintessential “network disease”: despite diverse etiologies (e.g., genes, acquired brain injuries), patients display consistent electroclinical features that are expressed via common brain networks. Our electroencephalography-functional

View this article online at [wileyonlinelibrary.com](https://onlinelibrary.wiley.com/doi/10.1002/ana.26368). DOI: 10.1002/ana.26368

Received Jan 19, 2022, and in revised form Mar 18, 2022. Accepted for publication Apr 11, 2022.

Address correspondence to Dr Warren, Melbourne Brain Centre, 245 Burgundy Street, Heidelberg, Vic, Australia 3084. E-mail: [aaron.warren@unimelb.edu.au](mailto:aaron.warren@unimelb.edu.au)

From the <sup>1</sup>Department of Medicine (Austin Health), University of Melbourne, Heidelberg, Vic, Australia; <sup>2</sup>Murdoch Children’s Research Institute, Parkville, Vic, Australia; <sup>3</sup>Florey Institute of Neuroscience and Mental Health, Heidelberg, Vic, Australia; <sup>4</sup>Department of Neurology, Austin Health, Heidelberg, Vic, Australia; <sup>5</sup>Bionics Institute, East Melbourne, Vic, Australia; <sup>6</sup>Department of Neurosurgery, Austin Health, Heidelberg, Vic, Australia; and <sup>7</sup>Department of Surgery, University of Melbourne, Parkville, Vic, Australia

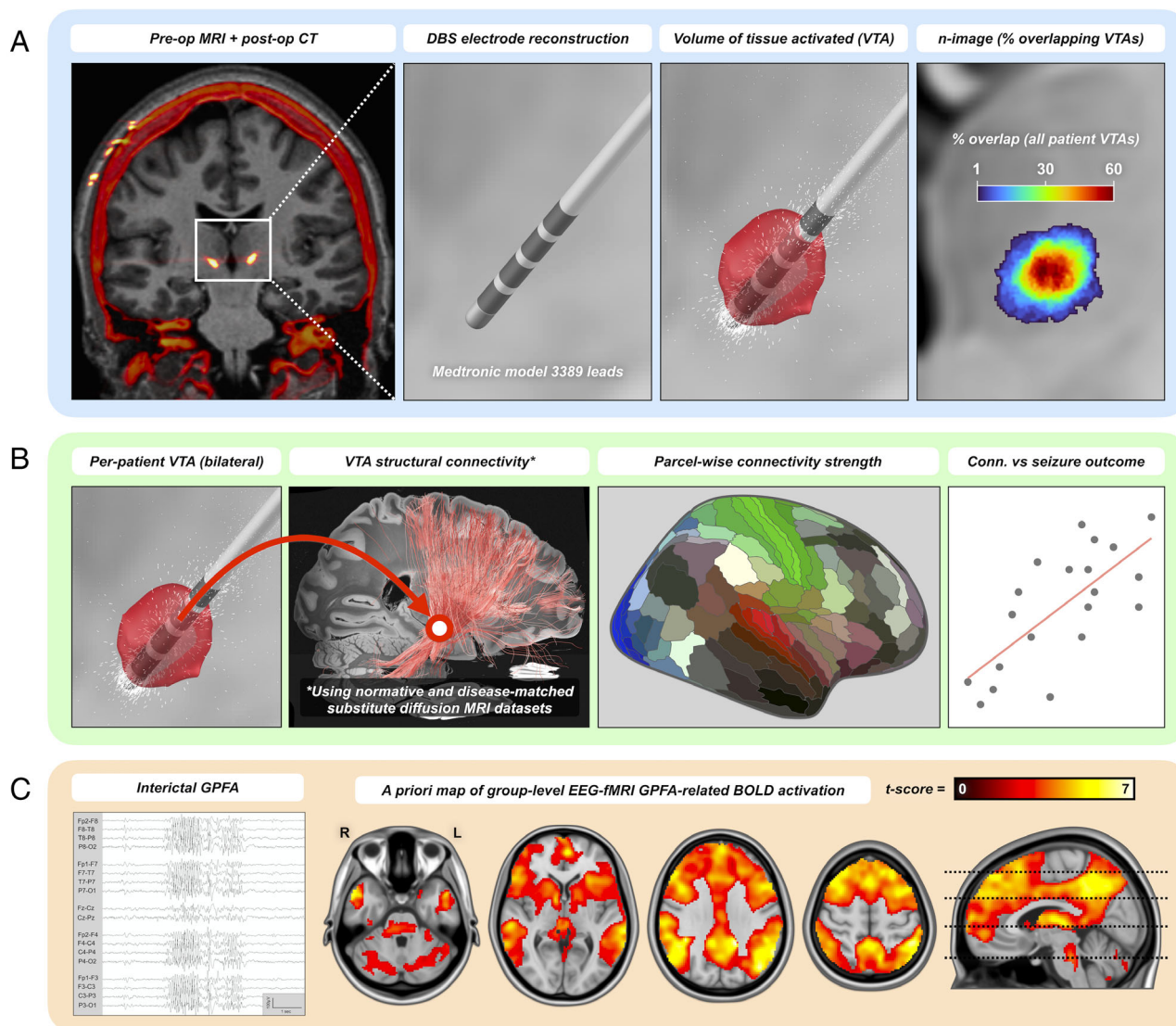


**FIGURE 1:** Overview of key imaging analysis steps. (A) Derivation of volumes of tissue activated (VTAs), representing the location and influence of DBS on surrounding tissue. DBS leads (Medtronic model 3389) were reconstructed by aligning post-operative CT to pre-operative MRI. Contact positions and stimulation settings were used to estimate bilateral VTAs.<sup>1, 19</sup> VTAs from all patients defined an *n*-image showing areas of overlap. Voxels with >20% overlap were analyzed to identify areas of above-mean (“sweet-spot”) and below-mean (“cold-spot”) seizure reduction. (B) VTAs were submitted to structural connectivity analyses using two “substitute” diffusion MRI datasets (a normative dataset of healthy subjects<sup>21</sup> and a “disease-matched” dataset of LGS patients from our previous imaging research<sup>5</sup>). Connectivity strength was calculated between bilateral VTAs and a custom, 429-region brain parcellation (available to view/download in NIfTI format: <https://identifiers.org/neurovault.collection:11930>). For each region, associations between connectivity and seizure outcomes were determined. (C) VTA connectivity was calculated to areas of known epileptic involvement in LGS, as defined by our previous combined EEG-functional MRI (EEG-fMRI) study of interictal generalized paroxysmal fast activity (GPFA) in 25 patients.<sup>5</sup> This yielded a map of group-level GPFA-related activation, displayed as *t*-scores thresholded at  $p < 0.05$  (corrected for family-wise error following threshold-free-cluster-enhancement<sup>5</sup>). The positions of axial slices are indicated by the dotted black lines on the sagittal view. Abbreviations: BOLD = blood-oxygen-level-dependent; EEG-fMRI = combined electroencephalography with functional magnetic resonance imaging; GPFA = generalized paroxysmal fast activity; VTA = volume of tissue activated.

MRI (EEG-fMRI) research showed that the brain areas generating epileptic activity are similar across patients with diverse causes of LGS, including thalamus, putamen, brainstem, and frontoparietal cortex (Figure 1C).<sup>5,6</sup> Hence, therapies capable of modulating this shared network, such as DBS, may be effective.<sup>7</sup>

Several DBS studies have been performed in LGS,<sup>8–11</sup> most recently including our randomized controlled trial<sup>12</sup> (named ESTEL: *Electrical Stimulation of Thalamus for Epilepsy of Lennox–Gastaut phenotype*) of bilateral DBS to the thalamic centromedian nucleus (CM). A key strength of ESTEL was the collection of

multiple seizure outcome measures (diaries and EEG), which sought to mitigate well-described concerns<sup>13</sup> about the accuracy of patient/caregiver diaries for documenting seizures in epilepsy treatment trials.

ESTEL offers unique opportunities to examine imaging predictors of CM-DBS outcome. However, outcome prediction in LGS presents challenges not commonly found in other diseases. Patients' clinical histories are highly diverse, with many having distorted neural anatomy due to injuries, malformations, or interventions before DBS (e.g., resective or disconnective surgeries).<sup>4</sup> There are also logistical obstacles to acquiring advanced pre-operative MRI in LGS, due to cognitive impairment and safety requirements (e.g., patients often have MRI-conditional devices *in situ*, including vagal nerve stimulators [VNS]). Furthermore, it typically takes several months (or even years)<sup>14</sup> to determine the full benefit of DBS, given the intermittent nature of seizures; this contrasts with conditions such as Parkinson's disease where efficacy is apparent soon after DBS is activated.<sup>15</sup>

Some of these obstacles may be circumvented by "normative" analysis approaches,<sup>3</sup> where patients' outcomes are predicted using connectivity patterns derived from healthy control MRI scans. Although these methods make assumptions about the relevance of control brains to patient outcomes, several studies have shown promising predictions of DBS efficacy.<sup>3,16,17</sup> For example, one study in Parkinson's disease found similar prediction accuracy when using scans from either healthy controls, a disease-matched group of patients who did not undergo DBS, or the participating patients themselves.<sup>17</sup>

Using outcome data from ESTEL,<sup>12</sup> we aimed to identify thalamic stimulation sites and brain connectivity patterns associated with seizure reduction following CM-DBS in LGS. We hypothesized that beneficial DBS would map to a specific subregion of the thalamus and would correlate with thalamic structural connectivity to areas of EEG-fMRI activation we previously demonstrated to underlie epileptic activity in LGS.<sup>5,6</sup>

## Methods

### Thalamic Nomenclature

Diverse nomenclatures and parcellation schemes are used in the thalamic DBS literature. Here, we use the nomenclature of Krauth/Morel,<sup>18</sup> with one exception: we refer to the CM as "centromedian nucleus," whereas in Krauth/Morel's scheme this same nucleus is termed "centre médian." We chose to use the term "centromedian" because it is more widely used in the CM-DBS literature.<sup>8-12</sup> Importantly, the centromedian/centre médian nucleus (in posterior intralaminar complex) should not be

confused with the distinct yet similarly named "central medial" nucleus (in anterior intralaminar complex).<sup>18</sup> Note that the original Krauth/Morel atlas<sup>18</sup> is defined in Montreal Neurological Institute (MNI) 6<sup>th</sup> generation template space; we nonlinearly warped the atlas to MNI 2009b asymmetric template space to match the default template space used in Lead-DBS software.<sup>19</sup>

### Patients and Trial Design

Detailed information about patients and the ESTEL trial design is provided in our previous work.<sup>12</sup> Briefly, 20 young adults with LGS underwent DBS surgery at Austin Health in Melbourne, Australia. One patient was excluded due to a cerebral infection.<sup>12</sup> The final cohort included 19 patients (13 females, 6 males; mean age = 25 years). The study received institutional approval from the Austin Health Human Research Ethics Committee (approval number = HREC/16/Austin/139; Australian New Zealand Clinical Trials Registry number = ACTRN12621001233819). Parents or a responsible guardian provided written informed consent before any study-specific procedures commenced.

ESTEL comprised four phases, each lasting 3 months: a pre-implantation baseline phase, a pre-stimulation phase (3 months post-implantation, before randomization), a blinded stimulation phase, and an unblinded stimulation phase. Patients were randomized to treatment and control arms. All patients received a minimum 3 months of stimulation. For the treatment group, stimulation first occurred during the 3-month blinded phase, followed by a further 3-month unblinded stimulation. In contrast, the control group received no stimulation during the blinded phase, followed by 3 months of unblinded stimulation. For the current analysis, we measured outcomes after the first 3 months of stimulation only, regardless of whether this occurred blinded or unblinded. This was intended to facilitate analysis of outcomes in the full cohort by making stimulation duration the same across all patients. Importantly, seizure outcomes did not significantly differ between patients who received their 3 months of stimulation in a blinded versus unblinded fashion (Table 1). Note that this strategy deviates from the primary outcome analyses in ESTEL (which compared treatment and control subgroups during the blinded phase), and so seizure outcomes summarized here differ slightly from those we reported previously.<sup>12</sup>

### Clinical Measures

Seizure outcomes were measured using three methods (Figure 2): (i) monthly diaries, (ii) ambulatory 24-hour EEGs; and (iii) a composite measure calculated using the average of (i) and (ii). Change in diary-recorded seizures

TABLE 1. Associations Between Seizure Outcomes and Baseline Clinical Variables

Clinical Variable	Association with % Seizure Reduction (Diaries)		Association with % Seizure Reduction (EEG)		Association with % Seizure Reduction (Diary-EEG Average)	
	Test Statistic	p-Value	Test Statistic	p-Value	Test Statistic	p-Value
Age (years) <sup>a</sup>	$rho = 0.24$	0.33	$rho = -0.43$	0.08	$rho = -0.15$	0.56
Baseline ABAS-3 (cumulative raw score) <sup>a</sup>	$rho = 0.16$	0.52	$rho = -0.16$	0.53	$rho = -0.05$	0.86
Baseline seizure frequency (diaries) <sup>a</sup>	$rho = 0$	0.99	$rho = -0.16$	0.55	$rho = -0.17$	0.52
Baseline seizure frequency (EEG) <sup>a</sup>	$rho = 0.05$	0.85	$rho = -0.31$	0.22	$rho = -0.28$	0.27
Sex <sup>b</sup>	$U = 65$	0.70	$U = 42$	0.80	$U = 45$	1.0
First 3 months DBS delivered blinded vs unblinded <sup>b</sup>	$U = 96$	0.66	$U = 62$	0.37	$U = 67$	0.67
Active VNS <i>in situ</i> <sup>b</sup>	$U = 141$	0.96	$U = 90$	0.06	$U = 94$	0.16
Abnormal structural MRI <sup>b</sup>	$U = 86$	0.28	$U = 82$	0.96	$U = 74$	0.54
Previous corpus callosotomy <sup>b</sup>	$U = 135$	0.15	$U = 121$	0.70	$U = 114$	0.78
Previous resective neurosurgery <sup>b</sup>	$U = 160$	0.23	$U = 127$	0.29	$U = 123$	0.09

Note: Results are shown separately for each of three seizure outcomes (diary, EEG, and diary-EEG average).

<sup>a</sup>Associations with continuous clinical variable performed using two-tailed Spearman’s rank-correlations.

<sup>b</sup>Associations with binary categorical clinical variables performed using two-tailed Mann–Whitney *U* tests.

Abbreviations: ABAS-3 = Adaptive Behaviour Assessment System–Third Edition; VNS = vagal nerve stimulator.

was measured as the percentage difference between average monthly seizure frequency at baseline and monthly seizure frequency in the final month of 3 months stimulation.

Change in EEG seizures was measured as the percentage difference between baseline seizures and after 3 months of stimulation.<sup>12</sup>

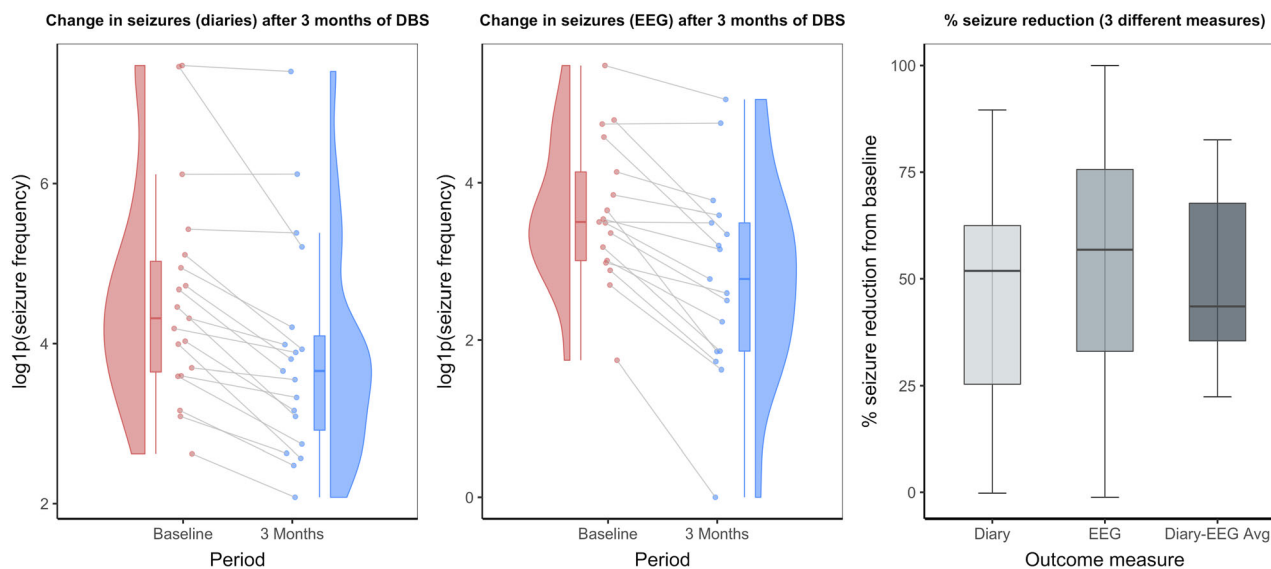


FIGURE 2: Seizure outcomes after 3 months of CM-DBS. Left and middle panels show per-patient change (gray lines) in seizure frequency (log1p transformed) between the pre-implantation baseline and after 3 months of active DBS for monthly diary and 24-hour EEG outcome measures, respectively. Boxplots in the right panel show the median (and interquartile range) percentage seizure reduction, relative to baseline, for the diary and EEG measures, and for the diary-EEG composite outcome measure (defined using the average of each patient’s diary and EEG percentage seizure reductions). [Color figure can be viewed at [www.annalsofneurology.org](http://www.annalsofneurology.org)]

In ESTEL, some discrepancy was found between diary and EEG outcomes, with the latter appearing to be a more sensitive marker of DBS benefit.<sup>12</sup> To capture each patient's overall change, for the current analysis we defined a composite outcome as the average percentage seizure reduction across diaries and EEG. For example, if a patient showed 40% reduction in diary seizures and 60% reduction in EEG seizures, then their diary-EEG average seizure reduction would be  $(40 + 60)/2 = 50\%$ . Due to the coronavirus disease 2019 (COVID-19) pandemic, 2 patients did not have ambulatory EEG recordings acquired at all timepoints.<sup>12</sup> Hence, EEG and diary-EEG average outcomes were assessed in 17/19 patients only.

To explore whether standard clinical variables were associated with outcomes (Table 1), we also recorded the following baseline information: age, sex, presence/absence of an *in situ* and active VNS device, presence/absence of structural MRI brain abnormalities (e.g., cortical malformations), presence/absence of previous resective neurosurgery (e.g., corticectomy), presence/absence of previous corpus callosotomy, baseline average monthly seizure frequency (diaries), baseline 24-hourly seizure frequency (EEG), and baseline adaptive behavior/disability measured using each patient's cumulative raw score on the *Adaptive Behavior Assessment System—Third Edition* (ABAS-3).<sup>12</sup>

### **DBS Implantation and Volumes of Tissue Activated**

Bilateral CM-DBS implantation (quadripolar Medtronic model 3389 leads) was performed using our previously described targeting approach,<sup>20</sup> guided by pre-operative structural MRI. To confirm DBS lead positions, a CT brain scan was acquired up to 1 day post-operatively. The CT was co-registered with the pre-operative MRI using Lead-DBS software version 2.5.2,<sup>19</sup> incorporating a correction for potential post-operative brain-shift. Lead trajectories and contact positions were then reconstructed from the CT.<sup>19,20</sup> To visualize positions in a common space, nonlinear warps were calculated<sup>20</sup> between patients' pre-operative MRI and MNI 2009b asymmetric space using Advanced Normalization Tools software. Voxel coordinates and anatomical locations of all DBS electrode contacts (4 per brain side) are provided for each patient in Supplementary Material available online: <https://osf.io/jtnwd>.

The volume of tissue activated (VTA) is an estimate of the effects of stimulation on surrounding tissue (Figure 1A).<sup>19</sup> Bilateral VTAs were computed for each patient using the stimulation parameters administered for the majority of their first 3-month stimulation period. Parameters for each patient were as described previously,<sup>12</sup>

with typical settings being: bilateral 2.5 V monopolar stimulation using the most centrally located contact within the CM, 90  $\mu$ s pulse width, 145 Hz, continuous duty-cycling (1 min on/5 mins off). VTAs were estimated using the finite element method (FEM)-based FieldTrip-SimBio pipeline in Lead-DBS.<sup>19</sup> Like previous studies,<sup>1,19</sup> VTAs were modelled assuming a homogenous tissue conductivity of 0.1 S/m and were thresholded to binary three-dimensional volumes by applying an electric field cutoff of 0.2 V/mm. All VTAs were generated in MNI space.

### **Probabilistic Stimulation Mapping**

Patient VTAs were used to define probabilistic maps showing thalamic subregions where stimulation yielded above-mean ("sweet-spots") and below-mean ("cold-spots") seizure reduction. Three maps were generated, one for each of the three outcome measures (diaries, EEG, diary-EEG average). This was achieved in four steps using methods described by Elias et al.,<sup>1</sup> in Lead-DBS.<sup>19</sup> First, to increase statistical power,<sup>19</sup> all right-sided VTAs were non-linearly flipped to the left hemisphere, yielding  $n \times 2$  left-sided VTAs (i.e., 2 per patient). Second, VTAs were weighted by each patient's percentage seizure reduction. These weights were demeaned and normalized by VTA size to penalize larger and less focal VTAs.<sup>1</sup> Third, to ensure the validity of voxel-wise statistics, only voxels common to >20% of VTAs were retained (Figure 1A).<sup>1</sup> Last, using the per-patient outcome-weighted VTAs, a two-tailed Wilcoxon signed-rank test was performed at each voxel, with the null hypothesis equal to the mean seizure reduction across the cohort. This yielded voxel-wise  $p$ -value maps expressing the degree of confidence that stimulation at a given voxel was associated with above-mean or below-mean seizure reduction.<sup>1</sup> To identify peak sweet- and cold-spot coordinates (Table 2), we thresholded each map at  $p < 0.05$  and extracted  $x$ ,  $y$ , and  $z$  coordinates (in mm; MNI 2009b asymmetric space) corresponding to the center-of-gravity of the largest surviving voxel cluster.

### **Structural Connectivity**

To assess connectivity associated with seizure outcomes, VTAs were included in diffusion-weighted imaging (DWI)-based connectivity analyses (Figure 1B). These were performed separately for each of the three outcomes (diaries, EEG, diary-EEG average), using "substitute" DWI scans obtained from two sources: (i) a high-quality normative dataset of healthy adults from the Human Connectome Project (HCP),<sup>21</sup> and (ii) a clinical-quality disease-matched dataset of LGS patients from our previous research.<sup>5</sup>

TABLE 2. Peak Coordinates for Above-Mean (“Sweet-Spot”) and Below-Mean (“Cold-Spot”) Seizure Reduction

Seizure outcome	Peak Coordinates for Sweet-Spot (mm; MNI 2009b asymm. Template Space)			Peak Coordinates for Cold-Spot (mm; MNI 2009b asymm. Template Space)		
	<i>x</i>	<i>y</i>	<i>z</i>	<i>x</i>	<i>y</i>	<i>z</i>
Diaries	−12	−17.7	0.08	−10.6	−18.9	3.45
EEG	−13.3	−16.8	1.36	−8.19	−19.1	0.08
Diary-EEG average	−13.3	−17.1	1.28	−10.5	−18	3.65
Mean coordinates	−12.87	−17.2	0.91	−9.76	−18.67	2.39

Note: For each seizure outcome (diary, EEG, and diary-EEG average), three-dimensional mm coordinates in MNI 2009b asymmetric template space are provided for peak sweet- and cold-spot locations. *x*, *y*, and *z* sweet-spot coordinates match the sagittal, coronal, and axial views displayed in Figure 3, respectively. Mean coordinates (across outcomes) are in the bottom row. Note that coordinates are provided for the left hemisphere only because all right-sided stimulation locations were first non-linearly flipped to the left hemisphere for this analysis. Coordinates of bilateral DBS electrode contacts for each individual patient are provided in Supplementary Material available online: <https://osf.io/jtnwd>. Abbreviations: MNI = Montreal Neurological Institute.

- *Substitute normative connectome*: We used the “100 unrelated subjects” dataset from the HCP<sup>21</sup> (54 females and 46 males; mean age = 29 years). Acquisition and pre-processing are described elsewhere.<sup>21</sup> Briefly, multi-shell DWI was acquired on a Siemens 3T “Connectom Skyra” scanner and were downloaded as “minimally pre-processed” data, having undergone corrections for motion and echoplanar imaging (EPI)/eddy current distortion, and co-registration with each subject’s T1-weighted scan. We performed further processing using MRtrix3<sup>22</sup> and MRtrix3Tissue<sup>23</sup> (<https://3Tissue.github.io>). Briefly, the following was performed in each subject’s native brain space: (i) up-sampling of DWI to 1 mm<sup>3</sup>, (ii) calculation of fiber orientation distribution (FOD) images using multi-shell multi-tissue constrained spherical deconvolution (CSD) and group-averaged “Dhollander” tissue response functions (white matter, gray matter, CSF)<sup>22</sup>; (iii) global intensity normalization of subject-specific FOD images; (iv) whole-brain probabilistic tractography (20 million streamlines) using iFOD2,<sup>22</sup> hybrid surface-volume anatomically constrained tractography (ACT),<sup>24</sup> and dynamic seeding; and (v) streamline weighting using spherically informed filtering of tractograms (SIFT2).<sup>25</sup>

The resulting SIFT2-weighted tractograms were used to calculate structural connectivity between patient VTAs and a custom, 429-region parcellation (available to view/download in NIFTI format: <https://identifiers.org/neurovault.collection:11930>) combining four brain atlases, together covering cortical and subcortical gray matter outside the thalamus: (i) HCPMMP1/Glasser cortical atlas,<sup>26</sup> (ii) 3T Scale IV Melbourne Subcortex Atlas<sup>27</sup> (edited to remove thalamus), (iii) Harvard

Ascending Arousal Network Atlas of brainstem nuclei,<sup>28</sup> and (iv) subject-specific segmentation of cerebellar lobules performed using volBrain/CERES.<sup>29</sup> Connectivity was defined as the sum of SIFT2 weights of all streamlines connecting region pairs, multiplied by SIFT2’s subject-specific fiber density proportionality coefficient (*mu*).<sup>25</sup> This yielded a 1x429 connectivity vector for each VTA. To account for differences in VTA volume, each vector was normalized by its total connection strength.<sup>16</sup> This process was repeated 100 times per VTA (i.e., once per HCP subject). The results were averaged across HCP subjects to create a 1x429 average connectivity vector per VTA. To create a bilateral connectivity vector per patient, HCP subject-average connectivity vectors corresponding to left and right VTAs were summed.<sup>16</sup> Finally, at each region, associations between connectivity strength and seizure outcomes were measured using Spearman’s rank-correlations.<sup>17</sup>

- *Substitute disease-matched connectome*: DWI data from 14 patients with LGS (none of whom participated in ESTEL) were selected from our previous neuroimaging research<sup>5</sup> (10 females, 4 males; mean age = 10 years). These patients were younger than the ESTEL cohort, but all had an electroclinical diagnosis of LGS and were recruited as per previously described protocols.<sup>5</sup> For the current analysis, we only included patients without prior neurosurgery or major structural brain abnormalities. Single-shell ( $+b = 0$ ) DWI was acquired on a 3T Siemens Trio scanner (2.3 mm<sup>3</sup> voxels; repetition time [TR]/echo time [TE] = 8,000/112 ms; 60 gradient directions with  $b = 3,000$  diffusion weighting and 7 directions without diffusion weighting [ $b = 0$ ]). A

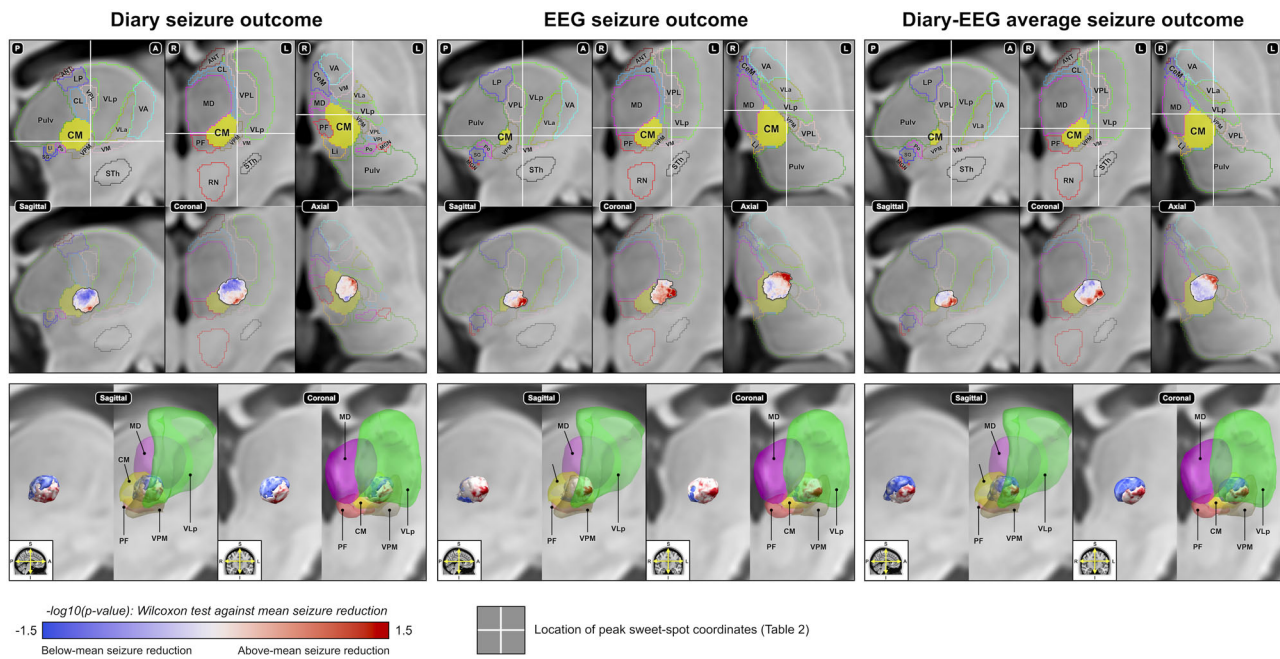


**FIGURE 3: Probabilistic stimulation mapping results.** For each seizure outcome (diary, EEG, and diary-EEG average), two-dimensional (upper panel) and three-dimensional (lower panel) views showing areas of above-mean (“sweet-spot”; pink-red areas) and below-mean (“cold-spot”; light blue-blue areas) seizure reduction, and their relationship to nearby thalamic anatomy, including the centromedian nucleus (CM; area in yellow). Results are displayed as  $-\log_{10}(p\text{-values})$  following a two-tailed Wilcoxon test against the mean seizure reduction at each voxel; values  $>1.301$  and  $<-1.301$  correspond to  $p\text{-values} < 0.05$ . Results can be viewed/downloaded in Nifti format: <https://identifiers.org/neurovault.collection:11930>. The white crosshairs indicate the location of peak sweet-spot coordinates provided in Table 2. Results are displayed in MNI 2009b asymmetric template space. Thalamic atlas overlay and nomenclature follows Krauth/Morel conventions.<sup>18</sup> Note that results are provided for the left hemisphere only because all right-sided stimulation locations were first non-linearly flipped to the left hemisphere for this analysis. Abbreviations: ANT = anterior nuclear group; CM = centromedian nucleus; CeM = central medial nucleus; CL = central lateral nucleus; Li = limitans nucleus; LP = lateral posterior nucleus; MD = mediodorsal nucleus; MGN = medial geniculate nucleus; Po = posterior nucleus; PF = parafascicular nucleus; Pulv = pulvinar nucleus; RN = red nucleus; SG = supragenicular nucleus; STh = subthalamic nucleus; VA = ventral anterior nucleus; VLa = ventral lateral nucleus (anterior subdivision); VLp = ventral lateral nucleus (posterior subdivision); VM = ventral medial nucleus; VPI = ventral posterior inferior nucleus; VPL = ventral posterior lateral nucleus; VPM = ventral posterior medial nucleus.

T1-weighted scan was also acquired. DWI pre-processing and VTA structural connectivity analysis followed all steps described above for the HCP dataset, with the following exceptions due to differences in DWI acquisition: (i) EPI distortion correction was performed without field-map or reverse phase-encoding data, using the “synthetic b0” approach implemented by Synb0-DISCO software<sup>30</sup>; and (ii) FOD images were generated using Single-Shell 3-Tissue CSD,<sup>23</sup> rather than multi-shell multi-tissue CSD.<sup>22</sup>

### Structural Connectivity to Areas of a Priori EEG-fMRI Activation

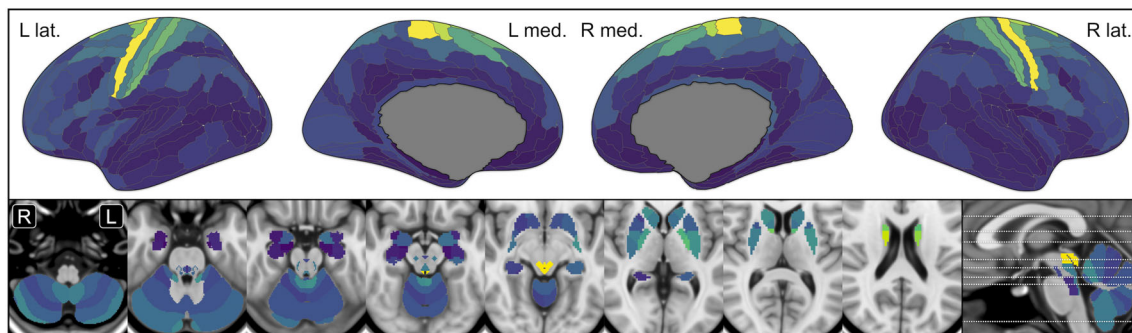
Our previous study<sup>5</sup> used combined EEG-fMRI in 25 LGS patients to reveal brain areas active during generalized paroxysmal fast activity (GPFA), a type of interictal epileptiform discharge characteristic of LGS and linked to tonic seizures.<sup>4</sup> This resulted in a spatial map of group-level GPFA-related EEG-fMRI activation (Figure 1C). In the current study, we tested whether seizure outcomes

after DBS are associated with VTA connectivity to these areas of known GPFA involvement. This was performed in two steps, using the connectomes calculated above. First, we identified regions within the 429-region parcellation showing a positive association ( $rho > 0$ ) with seizure outcomes. From these, we retained only regions where  $\geq 50\%$  of voxels overlapped with the EEG-fMRI map. Second, we summed connectivity strengths across all retained regions, yielding one value per patient representing total connectivity strength between their bilateral VTAs and areas of GPFA-related activation. This was repeated for each seizure outcome (diaries, EEG, diary-EEG average) and connectome type (normative, disease-matched).

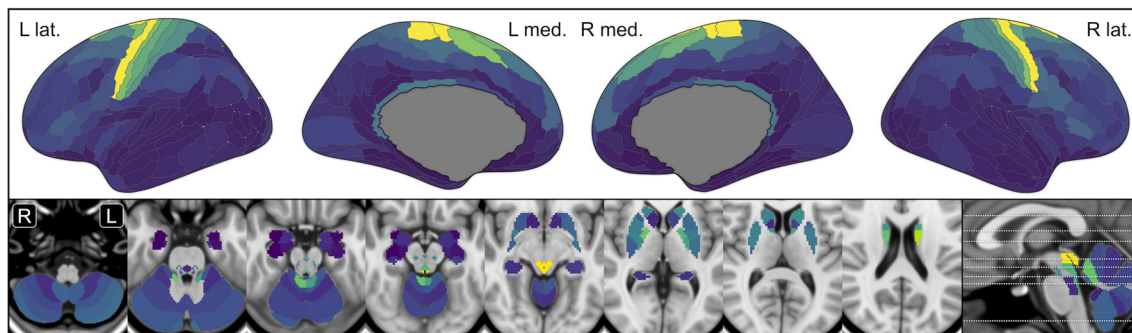
### Statistical Analyses

Statistical analyses were performed in MATLAB software version R2020b. All analyses were repeated separately for each of the three seizure outcomes (diaries, EEG, diary-EEG average). Associations between seizure outcomes and

## Normative substitute connectome



## Disease-matched substitute connectome



$\sqrt{\text{subject-average structural connectivity from bilateral VTAs}}$

0 0.25

**FIGURE 4:** Structural connectivity strength from bilateral VTAs. For the normative (upper row) and disease-matched (lower row) substitute connectome analyses separately, average structural connectivity strengths (across all patients' bilateral VTAs) are shown. For display purposes, connectivity strengths were first square root transformed to better distinguish areas of high/low connectivity. Results are displayed using a custom 429-region parcellation which can be viewed/downloaded in NIfTI format: <https://identifiers.org/neurovault.collection:11930>. Cortical hemisphere views were generated using *ggsegGlasser* software: <https://github.com/ggsegGlasser>. Positions of subcortical axial views are indicated by the dotted white lines on the sagittal view. Abbreviations: VTA = volume of tissue activated.

clinical variables (Table 1) were performed using two-tailed Mann–Whitney  $U$  tests for binary categorical variables (e.g., comparing % seizure reduction between patients with and without prior corpus callosotomy) and two-tailed Spearman's rank-correlations for continuous variables (e.g., correlating % seizure reduction with baseline ABAS-3 scores). For the normative and disease-matched analyses separately, associations between seizure outcomes and summed structural connectivity to areas of GPFA-related EEG-fMRI activation were performed using one-tailed Spearman's rank-correlations (i.e.,  $\rho > 0$ , given these analyses included only connectivity values from areas positively associated with outcomes). In each analysis, significance was assessed using an alpha of 0.05.

## Results

### Seizure Outcomes and Association with Clinical Variables

Across all patients, median percentage seizure reduction (relative to baseline) after 3 months of DBS was 52%

(range =  $-0.2$ –90%), 57% (range =  $-1$ –100%), and 44% (range = 22–83%) when measured using diaries, EEG, and diary-EEG average respectively (Figure 2).

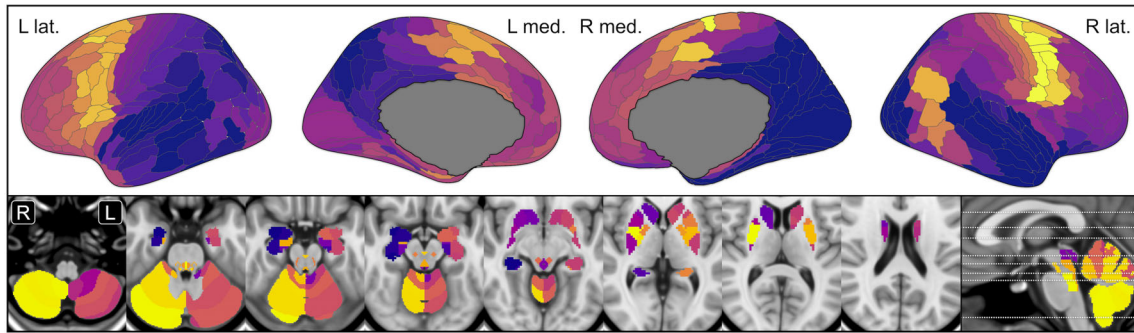
Table 1 displays associations between seizure outcomes and baseline clinical variables. No significant associations were found (all  $p > 0.05$ ).

### Probabilistic Stimulation Mapping

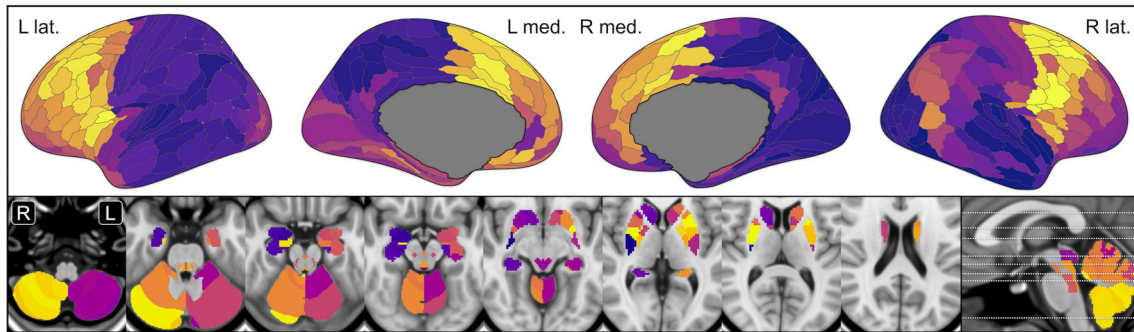
Locations where DBS tended to produce above-mean and below-mean seizure reduction are shown in Figure 3, while peak coordinates (in MNI space) are provided in Table 2. Results were similar across the three seizure outcomes. Above-mean seizure reduction was concentrated in the anterior, inferior, and lateral border of the CM, extending into the adjacent ventral lateral and ventral posterior medial nuclei. In contrast, below-mean seizure reduction was seen more medially, posteriorly, and superiorly, in the direction of the CM's borders with the parafascicular (PF), anterior pulvinar, and mediodorsal nuclei, respectively.



## Normative substitute connectome (association with diary-EEG avg seizure outcome)



## Disease-matched substitute connectome (association with diary-EEG avg seizure outcome)



Spearman correlation (bilat. VTA connectivity vs % seizure reduction)  
-0.5 0.5

**FIGURE 5: Associations between connectivity strength and diary-EEG average seizure outcome. For the normative (upper row) and disease-matched (lower row) substitute connectome analyses separately, associations between structural connectivity strength and the diary-EEG average seizure outcome are shown as Spearman's rank-correlations ( $\rho$ ). Orange-yellow colours indicate areas where connectivity strength was positively correlated with seizure reduction; pink-purple colours indicate areas where connectivity strength was negatively correlated with seizure reduction. Other display details as per Figure 4.**

Interestingly, when displayed upon the Krauth/Morel atlas,<sup>18</sup> peak sweet-spot coordinates for both the EEG and diary-EEG outcome measures (Table 2) were located *outside* the CM, within the posterior subdivision of the adjacent ventral lateral nucleus (Figure 3).

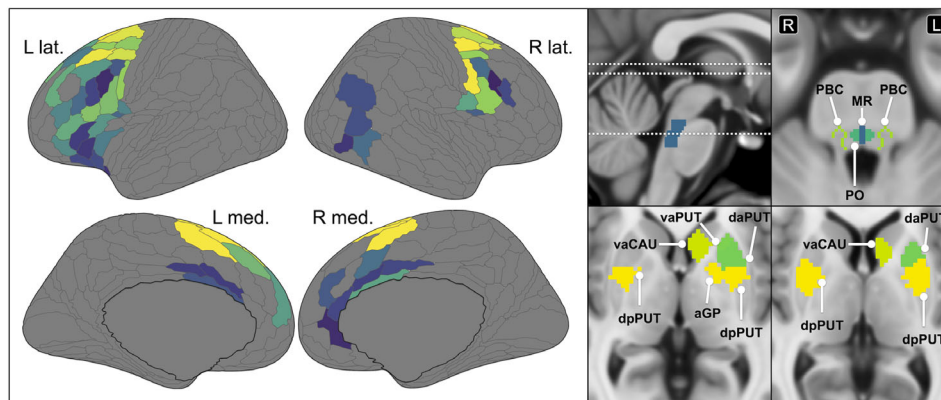
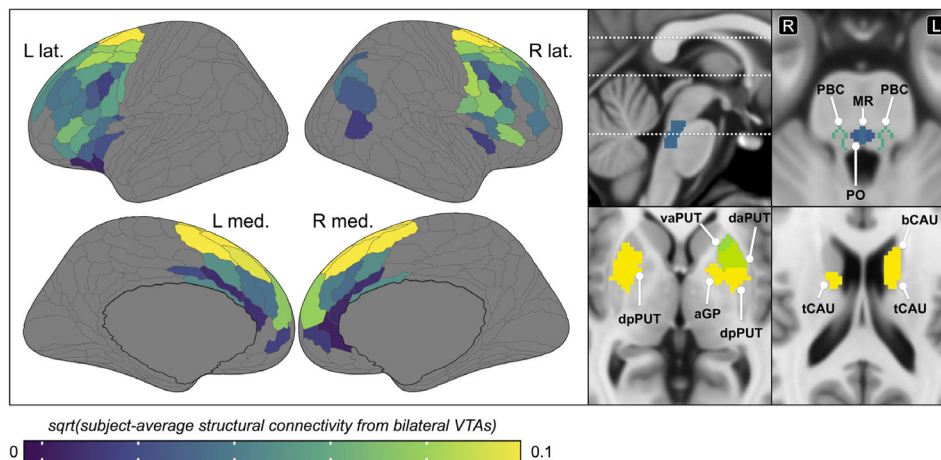
### Structural Connectivity

Average bilateral VTA structural connectivity strength is shown in Figure 4 for the normative and disease-matched substitute connectomes. Results were similar between connectome types and reflected the CM's known projections. Areas of strongest connectivity included pre- and post-central gyri, supplementary motor area, body/tail of the caudate, globus pallidus, anterior cerebellar vermis (lobule III), and the midbrain periaqueductal gray and reticular formation.

The association with seizure outcomes revealed a somewhat different pattern. Results were generally similar across the three seizure outcomes; therefore, we focus here on results for the diary-EEG average outcome, given this yielded the strongest correlation values (Figure 5). Seizure reduction was most positively correlated ( $\rho > 0.3$  across

both normative and disease-matched analyses) with connectivity to premotor cortex/Brodmann's area 6, frontal operculum, dorsoposterior putamen, globus pallidus, right hippocampal head, right inferoposterior cerebellum, and pontine locus coeruleus of the brainstem. In contrast, outcomes were most *negatively* correlated ( $\rho < -0.3$  across both normative and disease-matched analyses) with connectivity to medial and lateral temporal lobes, Heschl's gyrus/primary auditory cortex, occipital lobes, posterior insula, posterior cingulate, and much of posterior parietal cortex including precuneus and superior and inferior parietal lobules.

Figure 6 displays average connectivity strength for each area retained from the *a priori* map of GPFA-related EEG-fMRI activation. In both normative and disease-matched analyses, patients' sum of VTA connectivity to these areas showed a significant positive correlation with their diary-EEG average measure of seizure reduction (Figure 6). Similar trends were seen for the EEG (normative:  $\rho = 0.36$ ,  $p = 0.08$ ; disease-matched:  $\rho = 0.36$ ,  $p = 0.08$ ) and diary (normative:  $\rho = 0.23$ ,  $p = 0.17$ ; disease-matched:  $\rho = 0.33$ ,  $p = 0.08$ ) outcomes,

Normative substitute connectome (areas of *a priori* GPFA-related EEG-fMRI activation)Disease-matched substitute connectome (areas of *a priori* GPFA-related EEG-fMRI activation)

## Connectivity vs seizure reduction

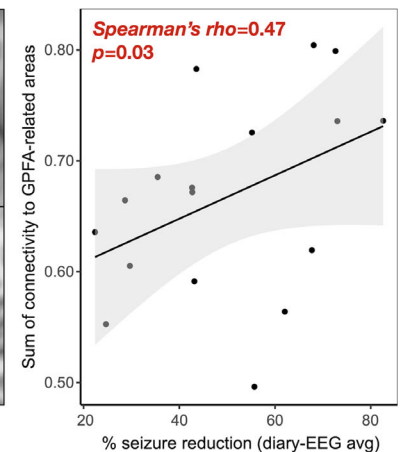
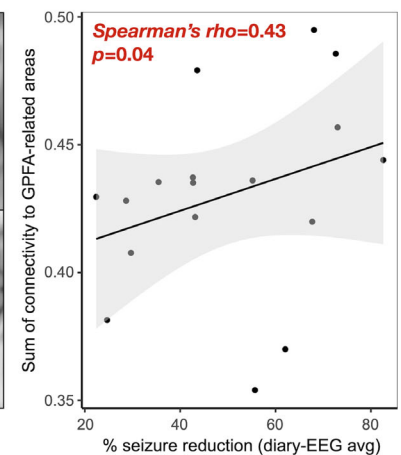


**FIGURE 6:** Structural connectivity to areas of *a priori* GPFA-related EEG-fMRI activation and association with diary-EEG average seizure outcome. For the normative (upper row) and disease-matched (lower row) substitute connectome analyses separately, average structural connectivity strength (across all patients' bilateral VTAs) is shown for select areas of *a priori* GPFA-related EEG-fMRI activation<sup>5</sup> defined by the map shown in Figure 1C. For display purposes, connectivity strengths were first square root transformed to better distinguish areas of high/low connectivity. Scatter plots on the right show the Spearman's rank-correlation ( $\rho$ ) between the diary-EEG average outcome and the sum of all connectivity strength to GPFA-related areas. The slope on each plot was fit by linear regression (gray shaded area = 95% confidence interval). Other display details as per Figure 4. Abbreviations: aGP = anterior globus pallidus; bCAU = caudate body; daPUT = dorsal anterior putamen; dpPUT = dorsal posterior putamen; GPFA = generalized paroxysmal fast activity; MR = median raphé nucleus; PBC = parabrachial complex; PO = pontis oralis; tCAU = caudate tail; vaCAU = ventral anterior caudate; vaPUT = ventral anterior putamen.

although the correlations were somewhat weaker and did not reach significance.

## Discussion

Our results indicate a potential sweet-spot for DBS in LGS, located in the anterior and inferolateral border of the CM and the adjacent ventral lateral nucleus (posterior subdivision). Additionally, seizure reduction is associated with connectivity to areas of EEG-fMRI activation we previously found to express epileptic activity in LGS,<sup>5</sup> including premotor and prefrontal cortex, putamen, and pontine brainstem. These findings suggest therapeutic mechanisms of CM-DBS and have implications for

planning future trials, optimizing stimulation in patients with existing devices, and developing new treatments.

### Optimal Target for CM-DBS

Our results confirm previous smaller studies, both in LGS<sup>8</sup> and a mixed epilepsy cohort,<sup>31</sup> suggesting anti-seizure effects of CM-DBS are maximal in the anterior and inferolateral CM, and raise the potential of a novel stimulation target for LGS in the form of the ventral lateral nucleus (posterior subdivision). The CM and its medial neighbor PF are commonly described—and targeted for DBS—as a unitary complex (“CM-PF”); however, in primates, the two nuclei are readily distinguishable with respect to their functions,<sup>32</sup>

cytoarchitectures,<sup>33</sup> and connectivity.<sup>34</sup> Finer subdivisions are less well-characterized, although histochemical analyses<sup>33</sup> separate CM into two components: a superomedial component containing larger neurons (“magnocellular CM”) and an inferolateral component containing smaller neurons (“parvocellular CM” or “CM proper”), the latter corresponding more to our observed sweet-spot. Precisely why DBS of parvocellular CM has greater anti-seizure effects remains to be determined; however, some clues may be found in the topography of the CM’s efferent projections. In axonal tracings of the primate thalamus,<sup>34</sup> the CM’s “lateral crescent” shows a high concentration of cortically projecting neurons, specifically projections to premotor and precentral cortex. This contrasts with medial CM locations, which show a higher number of striatally projecting neurons.<sup>34</sup>

Additionally, the parvocellular CM is known to innervate thalamocortical neurons in the adjacent ventral lateral nucleus, which similarly project to premotor cortex.<sup>34</sup> This may partly explain why the “peak” sweet-spot coordinates were surprisingly located outside the CM (Figure 3), within the posterior subdivision of the ventral lateral nucleus. A second possible explanation for this finding stems from the ventral lateral nucleus being the main thalamic pathway through which the cerebellum interacts with the cortex to support functions including motor control.<sup>35</sup> Early studies of epilepsy neuromodulation showed promising seizure reductions in patients with generalized epilepsy who underwent chronic cerebellar stimulation (see Kros et al.,<sup>35</sup> for a review). The thalamic ventral lateral nucleus may be an alternative way to modulate cerebellar output to the cortex and thus yield similar therapeutic benefits. Supporting this hypothesis is our recent observation of abnormal resting-state fMRI thalamocortical connectivity in LGS involving the ventral lateral nucleus.<sup>7</sup>

Therefore, one interpretation is that the parvocellular CM and ventral lateral nucleus may be optimal stimulation targets for LGS due to their preferential patterns of cortical/premotor connectivity and key positions within cerebello-thalamo-cortical pathways. However, the local influence of DBS likely extended several millimeters beyond these nuclei; thus, stimulation of adjacent structures may have also contributed to outcomes, either positively or negatively.

### **Optimal Connectivity for CM-DBS**

Seizure reduction was associated with connectivity to a cortico-subcortical circuit known to express epileptic activity in LGS. Our previous EEG-fMRI studies found a shared pattern of activation during GPFA,<sup>5</sup> which was similar across diverse causes of LGS.<sup>6</sup> This led to the

conceptualization of LGS as a “secondary network epilepsy,”<sup>6</sup> where the electroclinical syndrome is the expression of a common network that develops secondarily to the initiating cause, likely via complex interactions between neurodevelopmental processes, the underlying etiology, and recurrent epileptic activity during critical maturational periods. Hence, modulation of this shared network may be expected to have therapeutic effects across patients with diverse causes of LGS, consistent with what we observed here.

At the cortical level, structural connections to premotor and caudal prefrontal cortex were most positively associated with seizure reduction. In contrast, connections to posterior cortical areas (including parietal, occipital, and temporal lobes) tended to be negatively associated with outcomes. This suggests premotor and prefrontal cortex may have a key role in LGS, despite epileptic activity being characteristically generalized on scalp EEG.

Premotor cortex (approximately Brodmann area 6) is a transitional zone lying between prefrontal and primary motor cortex. Although not a uniform functional region,<sup>36</sup> premotor cortex is thought to contain multiple subdivisions involved in planning, learning, and executing complex actions including posture, gait, and reaching/grasping.<sup>36</sup> Several lines of evidence implicate this region in LGS. Direct premotor stimulation can elicit “negative” motor responses seen as a loss of axial and postural muscle tone,<sup>37</sup> echoing the clinical appearance of atonic “drop” seizures in patients with LGS.<sup>38</sup> Similarly, strokes and tumors restricted to premotor areas can cause paresis of shoulder movements associated with arm abduction and elevation,<sup>39</sup> again echoing the upper limb movements characteristically seen during generalized tonic seizures.<sup>38</sup> Our EEG-fMRI study using Dynamic Causal Modeling revealed a driving role of caudal middle frontal gyrus (encompassing premotor cortex) during interictal GPFA, with propagation occurring to the pontine brainstem and thalamus.<sup>5</sup> Finally, the diverse connectivity of premotor cortex, including to prefrontal and parietal cortex and the brainstem and spinal cord,<sup>36, 40</sup> is compatible with the diffuse EEG appearance of LGS and suggests premotor modulation is well-placed to influence a more extended epileptic network.

Subcortically, we found that connections to putamen and pontine brainstem were most consistently associated with benefit. The CM has strong modulatory effects on the striatum, particularly the putamen. In primates, chemical inactivation<sup>32</sup> and high-frequency (100 Hz) stimulation<sup>41</sup> of the CM inhibit putamen cholinergic interneurons, suggesting possible anti-seizure mechanisms. Regarding the brainstem, SPECT<sup>42</sup> and EEG-fMRI<sup>5</sup> studies have shown pontine activation during tonic seizures

and GPFA of LGS, consistent with the pons being an interface between cortico-reticular projections originating in premotor cortex<sup>43</sup> and descending reticulo-spinal tracts, which innervate truncal and proximal limb muscles involved in tonic seizures.<sup>38</sup> There is also emerging evidence that pontine stimulation may increase arousal responses in vegetative patients, possibly via engagement of the ascending reticular activating system.<sup>44</sup> Interestingly, we<sup>12</sup> and others<sup>45</sup> similarly observed increased arousal/alertness during CM-DBS, potentially reflecting engagement of this system.

A recent study by Torres Diaz et al.<sup>46</sup> of CM-DBS in 10 patients found some similarities to our results, including positive associations between diary-recorded seizure reduction and connectivity to premotor cortex and brainstem. However, several differences were also apparent. Torres Diaz et al. found that benefit was more positively associated with connections to primary motor and post-central sensory cortex than connections to basal ganglia including putamen; in contrast, we found the opposite (Figure 5). A possible explanation for this discrepancy may be differences in patients' epilepsy types. All patients in ESTEL underwent careful characterization including electroclinical diagnosis of LGS.<sup>12</sup> In contrast, patients in Torres Diaz et al. had various forms of "generalized epilepsy," with specific syndromes and EEG characteristics undefined. Given that the brain networks underlying generalized epileptic activity are known to differ between syndromes (e.g., between LGS<sup>5, 6</sup> and childhood absence epilepsy<sup>47</sup>), it is reasonable to postulate that connectivity markers of CM-DBS outcome may also be syndrome- or even seizure-specific. Hence, it is important for future studies to carefully define electroclinical diagnoses of included patients.

### Therapeutic Implications

LGS remains one of the most complex and challenging epilepsies to manage, and new treatment options are urgently needed. Current options<sup>4</sup> include various pharmacological therapies often administered in combination with resective neurosurgery (e.g., for patients who develop LGS secondary to a focal lesion<sup>6</sup>), corpus callosotomy, dietary therapies, and/or VNS. DBS is an efficacious<sup>12</sup> but still emerging addition to this treatment landscape, with significant unexplored potential to further optimize stimulation targets and parameters (e.g., frequency), and to perform direct comparisons of DBS efficacy to other therapies.

Our description of a sweet-spot may assist future DBS implantations for LGS, adding to a growing collection of similar sweet-spots for other conditions.<sup>1</sup> A second use may be optimizing patient programming, by selecting stimulation contact(s) nearest to our sweet-spot

coordinates. Additionally, our observation of specific connections associated with DBS benefit may inform development of other interventions and targets beyond the CM, including the recent concept of concurrent thalamic and cortical neuromodulation for LGS.<sup>48</sup>

Current methods for DBS targeting in epilepsy mostly rely on anatomical landmarks from pre-operative structural MRI<sup>8-12</sup>. However, our finding that outcomes are associated with connectivity to areas of EEG-fMRI activation suggests therapeutic benefits may be enhanced by tailoring stimulation targets using functionally defined epileptic zones or networks. These methods are already used in preoperative planning for other forms of epilepsy surgery (e.g., cortical resections for focal epilepsy tailored by EEG-fMRI<sup>49</sup>), and we anticipate that such information will improve patient-specific DBS targeting and efficacy.

Individual baseline clinical variables, including adaptive behavior/disability, did not show clear associations with seizure outcomes, at least within our modest sample size. This reflects other neuromodulation studies, including VNS for epilepsy<sup>50</sup> and DBS for Parkinson's disease,<sup>3</sup> where clinical factors showed either weak or broad (e.g., focal vs generalized seizures) associations with outcomes. The progressive way in which benefits of DBS appear to unfold<sup>14</sup> may be one explanation for the limited predictive power of baseline variables, given such progressive "network" changes are perhaps more strongly influenced by stimulation parameters, including targeting accuracy, than individual clinical factors. Alternatively, it is possible that clinical predictors are multifactorial or interact with stimulation parameters; however, this will require larger sample sizes to explore.

### Limitations and Future Directions

Accurate measurement of seizure outcomes for epilepsy DBS is challenging, particularly in LGS where parent/caregiver seizure diaries have numerous limitations.<sup>12</sup> ESTEL sought to mitigate this issue using ambulatory EEG recordings, which proved to be a more sensitive marker of seizure reduction.<sup>12</sup> In the current study, sweet-spot and connectivity results were generally similar between outcome measures; however, the strongest correlations were observed for the diary-EEG composite capturing each patient's "overall" benefit. This highlights the importance of precise outcome measurement for imaging and connectivity studies of epilepsy DBS. The emergence of "sensing" devices,<sup>48</sup> which automatically detect and log seizure activity, may be an effective strategy to enhance outcome accuracy.

ESTEL included patients with structural brain abnormalities and previous neurosurgery including corpus callosotomy,<sup>12</sup> which required a pragmatic analysis

approach. From an imaging/connectivity perspective, it would have been preferable to exclude such patients; however, this does not represent the LGS population, where >50% have structural brain abnormalities and many undergo other palliative procedures early in their clinical journey.<sup>4</sup> To circumvent this issue, we modeled connectivity using normative and disease-matched substitute DWI datasets, as in previous studies.<sup>3,16,17</sup> Although the largely ipsilateral nature of thalamic connections may be protective against bias due to corpus callosotomy, it is possible our results were influenced by inclusion of patients with previous neurosurgery. We anticipate that large, multi-center collaborations will be required to disentangle these factors, and to assess the predictive value of our findings at the individual patient level.

## Acknowledgments

We thank the patients and their families for participating. This work was supported by funding from the National Health and Medical Research Council (project grant #1108881). AELW was supported by a post-doctoral fellowship from the Lennox–Gastaut syndrome Foundation and an Early Career Researcher Grant from the University of Melbourne. LJD was supported by an Australian Government Research Training Program Scholarship. This research was supported by the University of Melbourne’s Research Computing Services and the Petascale Campus Initiative. Open access publishing facilitated by The University of Melbourne, as part of the Wiley - The University of Melbourne agreement via the Council of Australian University Librarians.

## Author Contributions

A.E.L.W., L.J.D., K.J.B., A.R., W.T., and J.S.A. contributed to the conception and design of the study; A.E.L.W., L.J.D., and J.S.A. contributed to acquisition and analysis of data; A.E.L.W., L.J.D., and J.S.A. contributed to drafting the text or preparing the figures.

## Potential Conflicts of Interest

A.E.L.W., L.J.D., and A.R. report no conflicts of interest relevant to this study. J.S.A. has received honoraria from Medtronic. K.J.B. and W.T. are co-founders and hold shares and options in Deep Brain Stimulation Technologies Pty Ltd and are named inventors on related patents. W.T. has also received honoraria from Medtronic and Boston Scientific.

## Data Availability

Code documenting our DWI pre-processing and connectivity analysis: <https://github.com/aeawarren/ESTEL-DBS>. Sweet-spot/cold-spot mapping results and our custom 429-region parcellation used for connectivity analyses are available to view/download in NIfTI format: <https://identifiers.org/neurovault.collection:11930>. Supplementary Material containing voxel coordinates and anatomical locations of all DBS electrode contacts for each patient: <https://osf.io/jtnwd>.

## References

1. Elias GJB, Boutet A, Joel SE, et al. Probabilistic mapping of deep brain stimulation: insights from 15 years of therapy. *Ann Neurol* 2021;89:426–443.
2. Horn A, Wenzel G, Irmen F, et al. Deep brain stimulation induced normalization of the human functional connectome in Parkinson’s disease. *Brain* 2019;142:3129–3143.
3. Horn A, Reich M, Vorwerk J, et al. Connectivity predicts deep brain stimulation outcome in Parkinson’s disease. *Ann Neurol* 2017;82:67–78.
4. Arzimanoglou A, French J, Blume WT, et al. Lennox-Gastaut syndrome: a consensus approach on diagnosis, assessment, management, and trial methodology. *Lancet Neurol* 2009;8:82–93.
5. Warren AEL, Harvey AS, Vogrin SJ, et al. The epileptic network of Lennox-Gastaut syndrome: cortically driven and reproducible across age. *Neurology* 2019;93:e215–e226.
6. Archer JS, Warren AEL, Stagnitti MR, et al. Lennox-Gastaut syndrome and phenotype: secondary network epilepsies. *Epilepsia* 2014;55:1245–1254.
7. Warren AEL, Abbott DF, Jackson GD, Archer JS. Thalamocortical functional connectivity in Lennox-Gastaut syndrome is abnormally enhanced in executive-control and default-mode networks. *Epilepsia* 2017;58:2085–2097.
8. Velasco AL, Velasco F, Jiménez F, et al. Neuromodulation of the centromedian thalamic nuclei in the treatment of generalized seizures and the improvement of the quality of life in patients with Lennox–Gastaut syndrome. *Epilepsia* 2006;47:1203–1212.
9. Valentín A, García Navarrete E, Chelvarajah R, et al. Deep brain stimulation of the centromedian thalamic nucleus for the treatment of generalized and frontal epilepsies. *Epilepsia* 2013;54:1823–1833.
10. Cukiert A, Burattini JA, Cukiert CM, et al. Centro-median stimulation yields additional seizure frequency and attention improvement in patients previously submitted to callosotomy. *Seizure* 2009;18:588–592.
11. Cukiert A, Cukiert CM, Burattini JA, Mariani PP. Seizure outcome during bilateral, continuous, thalamic centromedian nuclei deep brain stimulation in patients with generalized epilepsy: a prospective, open-label study. *Seizure* 2020;81:304–309.
12. Dalic LJ, Warren AEL, Bulluss KJ, et al. DBS of thalamic centromedian nucleus for Lennox-Gastaut syndrome (ESTEL trial). *Ann Neurol* 2022;91:253–267.
13. Hoppe C, Poepel A, Elger CE. Epilepsy: accuracy of patient seizure counts. *Arch Neurol* 2007;64:1595–1599.
14. Salanova V, Witt T, Worth R, et al. Long-term efficacy and safety of thalamic stimulation for drug-resistant partial epilepsy. *Neurology* 2015;84:1017–1025.

15. Deuschl G, Schade-Brittinger C, Krack P, et al. A randomized trial of deep-brain stimulation for Parkinson's disease. *N Engl J Med* 2006; 355:896–908.
16. Johnson KA, Duffley G, Anderson DN, et al. Structural connectivity predicts clinical outcomes of deep brain stimulation for Tourette syndrome. *Brain* 2020;143:2607–2623.
17. Wang Q, Akram H, Muthuraman M, et al. Normative vs patient-specific brain connectivity in deep brain stimulation. *Neuroimage* 2021;224:117307.
18. Krauth A, Blanc R, Poveda A, et al. A mean three-dimensional atlas of the human thalamus: generation from multiple histological data. *Neuroimage* 2010;49:2053–2062.
19. Horn A, Li N, Dembek TA, et al. Lead-DBS v2: towards a comprehensive pipeline for deep brain stimulation imaging. *Neuroimage* 2019;184:293–316.
20. Warren AEL, Dalic LJ, Thevathasan W, et al. Targeting the centromedian thalamic nucleus for deep brain stimulation. *J Neurol Neurosurg Psychiatry* 2020;91:339–349.
21. Glasser MF, Sotiropoulos SN, Wilson JA, et al. The minimal preprocessing pipelines for the human connectome project. *Neuroimage* 2013;80:105–124.
22. Tournier JD, Smith R, Raffelt D, et al. MRtrix3: a fast, flexible and open software framework for medical image processing and visualization. *Neuroimage* 2019;202:116137.
23. Dhollander T, Connelly A. A novel iterative approach to reap the benefits of multi-tissue CSD from just single-shell (+ b= 0) diffusion MRI data. *Paper presented at: 24th Annual Meeting of the International Society of Magnetic Resonance in Medicine*. ISMRM, Singapore; 2016:3010.
24. Mith R, Skoch A, Bajada CJ, et al. Hybrid surface-volume segmentation for improved anatomically-constrained tractography. *Paper presented at: 26th Annual Meeting of the Organization for Human Brain Mapping*. OHBM, Virtual Meeting, 2020:1034.
25. Smith RE, Tournier JD, Calamante F, Connelly A. SIFT2: enabling dense quantitative assessment of brain white matter connectivity using streamlines tractography. *Neuroimage* 2015;119:338–351.
26. Glasser MF, Coalson TS, Robinson EC, et al. A multi-modal parcellation of human cerebral cortex. *Nature* 2016;536:171–178.
27. Tian Y, Margulies DS, Breakspear M, Zalesky A. Topographic organization of the human subcortex unveiled with functional connectivity gradients. *Nat Neurosci* 2020;23:1421–1432.
28. Edlow BL, Takahashi E, Wu O, et al. Neuroanatomic connectivity of the human ascending arousal system critical to consciousness and its disorders. *J Neuropathol Exp Neurol* 2012;71:531–546.
29. Romero JE, Coupe P, Giraud R, et al. CERES: a new cerebellum lobe segmentation method. *Neuroimage* 2017;147:916–924.
30. Schilling K, Blaber J, Hansen C, et al. Distortion correction of diffusion weighted MRI without reverse phase-encoding scans or field-maps. *PLoS One* 2020;15:e0236418.
31. Son B-c, Shon YM, Choi J-g, et al. Clinical outcome of patients with deep brain stimulation of the Centromedian thalamic nucleus for refractory epilepsy and location of the active contacts. *Stereotact Funct Neurosurg* 2016;94:187–197.
32. Matsumoto N, Minamimoto T, Graybiel AM, Kimura M. Neurons in the thalamic CM-pf complex supply striatal neurons with information about behaviorally significant sensory events. *J Neurophysiol* 2001; 85:960–976.
33. Hirai T, Jones EG. A new parcellation of the human thalamus on the basis of histochemical staining. *Brain Res Brain Res Rev* 1989;14:1–34.
34. Sadikot AF, Parent A, Francois C. Efferent connections of the centromedian and parafascicular thalamic nuclei in the squirrel monkey: a PHA-L study of subcortical projections. *J Comp Neurol* 1992;315: 137–159.
35. Kros L, Eelkman Rooda OHJ, De Zeeuw CI, et al. Controlling cerebellar output to treat refractory epilepsy. *Trends Neurosci* 2015;38: 787–799.
36. Graziano MS, Taylor CS, Moore T, et al. The cortical control of movement revisited. *Neuron* 2002;36:349–362.
37. Luders H, Lesser RP, Dinner DS, et al. Localization of cortical function: new information from extraoperative monitoring of patients with epilepsy. *Epilepsia* 1988;29:556–565.
38. Gastaut H, Roger J, Ocjahchi S, et al. An electroclinical study of generalized epileptic seizures of tonic expression. *Epilepsia* 1963;4: 15–44.
39. Freund HJ, Hummelsheim H. Lesions of premotor cortex in man. *Brain* 1985;108:697–733.
40. Wise SP, Boussaoud D, Johnson PB, Caminiti R. Premotor and parietal cortex: corticocortical connectivity and combinatorial computations. *Annu Rev Neurosci* 1997;20:25–42.
41. Nanda B, Galvan A, Smith Y, Wichmann T. Effects of stimulation of the centromedian nucleus of the thalamus on the activity of striatal cells in awake rhesus monkeys. *Eur J Neurosci* 2009;29:588–598.
42. Intusoma U, Abbott DF, Masterton RA, et al. Tonic seizures of Lennox-Gastaut syndrome: Periictal single-photon emission computed tomography suggests a corticopontine network. *Epilepsia* 2013;54:2151–2157.
43. Jang SH, Lee SJ. Corticoreticular tract in the human brain: a mini review. *Front Neurol* 2019;10:1188.
44. Elias GJB, Loh A, Gwon D, et al. Deep brain stimulation of the brainstem. *Brain* 2021;144:712–723.
45. Martin RA, Cukiert A, Blumenfeld H. Short-term changes in cortical physiological arousal measured by electroencephalography during thalamic centromedian deep brain stimulation. *Epilepsia* 2021;62: 2604–2614.
46. Torres Diaz CV, Gonzalez-Escamilla G, Ciolac D, et al. Network substrates of Centromedian nucleus deep brain stimulation in generalized Pharmacoresistant epilepsy. *Neurotherapeutics* 2021;18: 1665–1677.
47. Carney P, Masterton R, Harvey A, et al. The core network in absence epilepsy differences in cortical and thalamic BOLD response. *Neurology* 2010;75:904–911.
48. Kwon CS, Schupper AJ, Fields MC, et al. Centromedian thalamic responsive neurostimulation for Lennox-Gastaut epilepsy and autism. *Ann Clin Transl Neurol* 2020;7:2035–2040.
49. Kowalczyk MA, Omidvarnia A, Abbott DF, et al. Clinical benefit of presurgical EEG-fMRI in difficult-to-localize focal epilepsy: a single-institution retrospective review. *Epilepsia* 2020;61:49–60.
50. Workewych AM, Arski ON, Mithani K, Ibrahim GM. Biomarkers of seizure response to vagus nerve stimulation: a scoping review. *Epilepsia* 2020;61:2069–2085.